

Generation of Spectral–Temporal Response Surfaces by Combining Multispectral Satellite and Hyperspectral UAV Imagery for Precision Agriculture Applications

Caroline M. Gevaert, Juha Suomalainen, Jing Tang, and Lammert Kooistra

Abstract—Precision agriculture requires detailed crop status information at high spatial and temporal resolutions. Remote sensing can provide such information, but single sensor observations are often incapable of meeting all data requirements. Spectral–temporal response surfaces (STRSs) provide continuous reflectance spectra at high temporal intervals. This is the first study to combine multispectral satellite imagery (from Formosat-2) with hyperspectral imagery acquired with an unmanned aerial vehicle (UAV) to construct STRS. This study presents a novel STRS methodology which uses Bayesian theory to impute missing spectral information in the multispectral imagery and introduces observation uncertainties into the interpolations. This new method is compared to two earlier published methods for constructing STRS: a direct interpolation of the original data and a direct interpolation along the temporal dimension after imputation along the spectral dimension. The STRS derived through all three methods are compared to field measured reflectance spectra, leaf area index (LAI), and canopy chlorophyll of potato plants. The results indicate that the proposed Bayesian approach has the highest correlation ($r = 0.953$) and lowest RMSE (0.032) to field spectral reflectance measurements. Although the optimized soil-adjusted vegetation index (OSAVI) obtained from all methods have similar correlations to field data, the modified chlorophyll absorption in reflectance index (MCARI) obtained from the Bayesian STRS outperform the other two methods. A correlation of 0.83 with LAI and 0.77 with canopy chlorophyll measurements are obtained, compared to correlations of 0.27 and 0.09, respectively, for the directly interpolated STRS.

Index Terms—Crop phenology, data fusion, hyperspectral imaging, image resolution, precision agriculture.

Manuscript received September 15, 2014; revised February 06, 2015; accepted February 11, 2015. This work was supported by the Smart Inspectors Project funded by the INTERREG IV A program Deutschland-Nederland.

C. M. Gevaert was with the Department of Physical Geography and Ecosystem Science, Lund University, SSE-223 62 Lund, Sweden. She is now with the Department of Earth Observation Science, Faculty ITC, University of Twente, 7500 AE Enschede, The Netherlands (e-mail: c.m.gevaert@utwente.nl).

J. Suomalainen is with the Laboratory of Geo-Information Science and Remote Sensing, Wageningen University, 6700 AA Wageningen, The Netherlands (e-mail: juha.suomalainen@wur.nl).

J. Tang is with the Department of Physical Geography and Ecosystem Science, Lund University, SE-223 62 Lund, Sweden (e-mail: lu.gistangjing@gmail.com).

L. Kooistra is with the Laboratory of Geo-Information Science and Remote Sensing, Wageningen University, 6700 AA Wageningen, The Netherlands (e-mail: lammert.kooistra@wur.nl).

Color versions of one or more of the figures in this paper are available online at <http://ieeexplore.ieee.org>.

Digital Object Identifier 10.1109/JSTARS.2015.2406339

I. INTRODUCTION

IN THE context of threatened global food security, precision agriculture is one strategy which can maximize yield to meet increased food demands, while minimizing the economic and environmental costs of food production [1]. Precision agriculture requires detailed information regarding temporal and spatial variations in crop conditions, which can be obtained through remote sensing [1]. The specific data requirements depend on the intended application. For example, the required spatial resolution could be 5–10 m for variable rate application of fertilizer, 1–3 m for crop biomass and yield prediction, and 0.5–1 m for weed control applications [2]. The required spectral resolution also depends on the application. Hyperspectral indices are capable of targeting reflectance at specific wavelengths for estimating chlorophyll [3], canopy nitrogen content [4], and carotenoids [5]. Narrowband vegetation indices obtained from hyperspectral data have been shown to obtain higher correlations to crop leaf area index (LAI) [6] and chlorophyll content [7] than broadband indices.

The use of satellite imagery to support agricultural applications has been recognized since the 1970s [2]. However, inadequate spatial and spectral resolutions as well as insufficient revisiting frequencies have largely impaired the use of satellite sensors for crop management [8]. Recently, some studies have shown that hyperspectral systems can be mounted on unmanned aerial vehicles (UAVs) [9]. The hyperspectral mapping system (HYMSY) developed at Wageningen University under the Smart Inspectors project [10] is one such example. Flexible image acquisition dates and user-controlled spatial resolution as well as flight paths are the benefits of such a system.

However, UAV image acquisition is also paired with high operational costs [9] which may therefore limit the number of high-resolution UAV images available. This is problematic, as the temporal dynamics of crop surface reflectance are important for crop monitoring and yield prediction applications [11], [12]. One solution is to supplement hyperspectral data with satellite observations at lower spectral resolutions. This could provide a more complete representation of the temporal dynamics of spectral reflectance, especially during growing seasons or compare relatively new hyperspectral data with historical satellite data to improve decision-making in precision agriculture [2].

Fusing images from two different sensors may provide datasets which exceed physical limitations of each individual

sensor. For example, Roy *et al.* [13] presented the spatial and temporal adaptive reflectance fusion model (STARFM), to fuse Landsat and MODIS imagery which allows the user to obtain synthetic imagery with a spatial resolution of 30 m at a daily interval. However, this method requires the two types of imagery at different spatial resolution to have corresponding spectral bands, and can be sensitive to temporal changes [14], [15] use unmixing-based techniques for spatial-temporal fusion, which eliminates the corresponding-band requirements in the STARFM method and allows for the downscaling of additional spectral bands from medium spatial resolution sensors. Similarly, Fasbender *et al.* [16] present a pan-sharpening approach with a Bayesian framework which compared favorably to other pan-sharpening methods. However, in the current application, the high-resolution imagery (hyperspectral UAV) has a higher spectral resolution than the medium-resolution imagery (multispectral Formosat-2). The motivation of the current study is to investigate methods which can retain valuable hyperspectral information from the UAV imagery and use additional information from multispectral observations to obtain a more complete temporal profile.

Two previous studies [17], [18] combined multiple sources of imagery to create a reflectance spectrum, continuous along both temporal and spectral domains. This creates a four-dimensional (4-D) dataset (latitude, longitude, wavelength, date) known in literature as a spectral-temporal response surface (STRS) [17] or spectral-temporal analysis by response surface [18]. The surfaces were formed by interpolating the reflectance of each pixel along the spectral and temporal dimensions. Mello *et al.* [18] utilized the polynomial trend surface (PTS) and collocation surface (CS) methods to combine Landsat-7/ETM+ and Landsat-5/TM imagery to differentiate between sugarcane harvest methods in Brazil. Villa *et al.* [17] focused on the development of an STRS methodological framework. Their study utilized a two-step interpolation technique: first interpolating MERIS and MODIS spectra along the wavelength dimension using a spline interpolation, and then interpolating along the temporal dimension.

However, these two approaches have a number of limitations. First, they do not account for the physical characteristics of reflectance spectra. Therefore, the interpolated spectra may be unrealistic, such as a missing red-edge for vegetation spectra. Second, all reflectance observations are weighted equally and the uncertainties of each measurement are not taken into account. Third, these studies combine two sensors with similar spectral characteristics. However, the current study combines multispectral satellite imagery with only four spectral bands with hyperspectral imagery (101 bands) from an UAV. The large differences between the spectral characteristics of both sensors make it more difficult to directly compare reflectance measurements.

To overcome these difficulties, the current study proposes a new methodology to obtain STRS based on Bayesian theory, which allows the uncertainties to be quantified [19]. First, the multispectral reflectance spectra are imputed to the hyperspectral intervals based on the *a priori* covariance between spectral bands of similar signatures. This causes the interpolated spectra to retain the physical features characteristic of vegetation

spectra, even when combining multispectral and hyperspectral images. Second, the temporal interpolation utilizes Bayesian inference and takes observation uncertainties into account.

The objective of this study is to present a new method to combine hyperspectral and multispectral imagery into STRS. This Bayesian method is compared to two other STRS methods based on [17] and [18]. All three methods are tested for a potato field in The Netherlands during the 2013 growing season. Extensive field measurements of crop reflectances, LAI, and canopy chlorophyll are utilized to evaluate the quality of the STRS results for the three methods.

II. THEORY

A. Spectral Interpolation: Bayesian Imputation

Hyperspectral observations of vegetation often present high correlations between spectral bands [20]. The current paper assumes that given the *a priori* covariance of hyperspectral bands, a hyperspectral reflectance spectrum can be inferred from the multispectral imagery using Bayesian imputation.

Suppose x_{m_i} represents the surface reflectance factor at the wavelengths of the multispectral sensor and x_{h_i} represents the unknown hyperspectral surface reflectance factors at date i . These distributions are jointly Gaussian defined by (1) with the marginal (2) and (3)

$$\mu = \begin{pmatrix} \mu_h \\ \mu_m \end{pmatrix}, \quad \Sigma = \begin{pmatrix} \Sigma_{hh} & \Sigma_{hm} \\ \Sigma_{mh} & \Sigma_{mm} \end{pmatrix} \quad (1)$$

$$p(x_h) = N(x_h | \mu_h, \Sigma_{hh}) \quad (2)$$

$$p(x_m) = N(x_m | \mu_m, \Sigma_{mm}) \quad (3)$$

Given the *a priori* mean (μ_m) and distribution (Σ_{mm}) of the multispectral reflectance factors and the covariance matrix Σ_{hh} of the hyperspectral reflectance data, the posterior conditional distribution (4) can be obtained by computing the model parameters described in (5) and (6) [19]

$$p(x_{h_i} | x_{m_i}) = N(x_{h_i} | \mu_{h|m}, \Sigma_{h|m}) \quad (4)$$

$$\mu_{(x_{h_i} | x_{m_i})} = \mu_h + \sum_{hm} \Sigma_{mm}^{-1} (x_m - \mu_m) \quad (5)$$

$$\Sigma_{(x_{h_i} | x_{m_i})} = \Sigma_{hh} - \sum_{hm} \Sigma_{mm}^{-1} \sum_{mh} \quad (6)$$

The estimation \hat{x}_{ij} of the missing spectral value is defined as the mean value of the posterior predictive presented in (4). It can be calculated as follows:

$$\hat{x}_{ij} = E[x_j | x_{m_i}, \theta] \quad (7)$$

where θ refers to the model parameters, and x_j refers to the reflectance at wavelength j .

Although hyperspectral bands display a high covariance between wavelengths, the nature of this covariance will vary depending on the surface properties, i.e., fractions of bare ground or vegetation. This implies that the covariance between

hyperspectral and multispectral wavelengths will vary according to different land cover types and must be calculated, accordingly. The current implementation selects a large number ($n = 100$) of hyperspectral signatures which are very similar to the multispectral signatures which are to be imputed. These observations are used to determine the covariance of the corresponding bands among two imagery sets. The selection of priors is further discussed in Section III-C.

B. Temporal Interpolation: Bayesian Inference

After obtaining the synthetic narrow band spectra of the multispectral observations, the Bayesian inference is utilized to interpolate along the temporal dimension to create the STRS. The method infers a vector of true spectral reflectance factors \mathbf{x} from a number of noisy observations \mathbf{y} . The mathematical formulation is set up as a linear Gaussian system (8)

$$\mathbf{y} = \mathbf{A}\mathbf{x} + \boldsymbol{\epsilon} \quad (8)$$

$$\boldsymbol{\epsilon} \sim N\left(0, \sum_{\mathbf{y}}\right), \quad \sum_{\mathbf{y}} = \sigma_{\mathbf{y}}^2 \mathbf{I} \quad (9)$$

where \mathbf{A} is a logical $N \times D$ matrix of the N number of observations and D is the length of the date vector which will be interpolated. This matrix \mathbf{A} is used to select the dates for which images are available. The noise is assumed to have normal Gaussian distribution (9) with a mean value of 0 and the distribution equal to the observation noise, or sensor precision ($\sigma_{\mathbf{y}}^2$) which is further multiplied by an identity matrix \mathbf{I} . The sensor precision is inversely related to the uncertainty and must be estimated by the user (see Section III-D).

The vector of true reflectance factors \mathbf{x} is also defined as a Gaussian distribution (10). The temporal profile is assumed to be smooth, meaning that the value of \mathbf{x} at date j is the average of its neighbors (11) altered by Gaussian noise (12)

$$p(\mathbf{y}|\mathbf{x}) = N\left(\mu_{\mathbf{y}|\mathbf{x}}, \sum_{\mathbf{x}}\right) \quad (10)$$

$$\mu_{\mathbf{y}|\mathbf{x}} = -\mathbf{L}^T \mathbf{L} \mathbf{x} \quad (11)$$

$$\sum_{\mathbf{x}} = (\sigma_{\mathbf{x}}^2 \mathbf{L}^T \mathbf{L})^{-1} \quad (12)$$

$$\mathbf{L} = \frac{1}{2} \begin{pmatrix} -1 & 2 & -1 & & \\ & \dots & & & \\ & & -1 & 2 & -1 \end{pmatrix} \quad (13)$$

where \mathbf{L} (13) is a second-order finite difference matrix used to control the error term as a function of the discrepancy between neighboring observations [19]. $\sigma_{\mathbf{x}}$ can be used to control the smoothness of the interpolation. By assigning the prior data a higher precision than the precision of the observations ($\sigma_{\mathbf{x}} > \sigma_{\mathbf{y}}$), the prior will have a higher weight in the interpolation, resulting in a smoother profile. Conversely, by assigning a relatively low $\sigma_{\mathbf{x}}$ ($\sigma_{\mathbf{x}} < \sigma_{\mathbf{y}}$), the temporal interpolation will more closely follow the observed spectra [19]. The value of $\sigma_{\mathbf{x}}$ depends on the expected variability of the spectra over time, and may be determined empirically. Section III-D explains how $\sigma_{\mathbf{x}}$ was obtained in the current study.

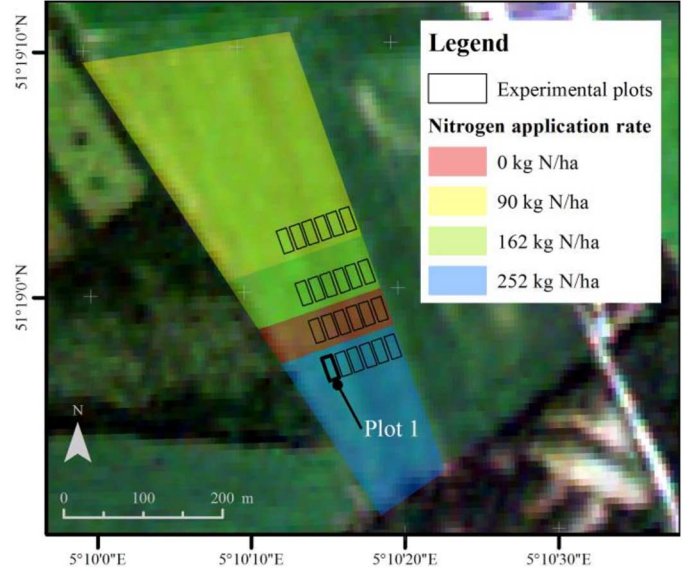


Fig. 1. Study area consisting of 24 experimental plots under four different initial fertilization regimes over the Formosat-2 image on July 18th.

The STRS is created by interpolating the spectral reflectance along the temporal dimension on a band-by-band basis. For each wavelength, the hyperspectral and imputed multispectral observations are selected, along with their corresponding uncertainties. The observations of the neighboring spectral bands are also utilized as input, but with a doubled uncertainty. In this way, although the temporal interpolation is applied separately for each band, the observations of neighboring bands restrain the interpolation.

III. METHODOLOGY

A. Study Area

The study area is a potato field at $51^{\circ}19'00''$ N and $05^{\circ}10'14''$ E, near the village of Reusel in The Netherlands. The average spectral reflectance with four levels of initial fertilization from 24 experimental plots (13×30 m) (Fig. 1) was obtained on a weekly basis between June 6, 2013 and August 23, 2013 (Table I). Six spectral measurements were taken per experimental plot using a CropsCan Multispectral Radiometer (MSR16R, CropsCan Inc.) which has 13 spectral bands in the VIS/NIR spectrum (Table I) [4]. At the same locations, an LAI-2000 Plant Canopy Analyzer was used to measure the LAI of potato plants and a Minolta SPAD-502 was used to obtain chlorophyll measurements after transforming SPAD values to chlorophyll concentrations using the relations described by [21]. More information regarding the experimental setup can be found in [21].

B. Image Pre-Processing

A hyperspectral system on an UAV consisting of a Specim ImSpector V10 2/3'' spectrograph mounted on an Aerialtronics Altura AT8 octocopter was developed by the WU under the Smart Inspectors project [10]. This UAV was flown over the

TABLE I
CHARACTERISTICS OF DATASETS USED IN THE PRESENT STUDY

	UAV	FORMOSAT-2	CROPSCAN
Spatial resolution	1 m	8 m	–
No. of bands	101	4	13
Center wavelength	Every 5 nm between 450 nm and 900 nm	485, 560, 660, and 830 nm	490, 530, 550, 570, 670, 700, 710, 740, 750, 780, 870, 940, and 950 nm
Acquisition dates	June 6, 14 July 5, 17	April 24 June 6, 8 July 2, 8, 18, 22 August 2	June 6, 14, 21, 26 July 5, 12, 17, 26, 31 August 16, 23

study area at four dates (Table I). All images were georeferenced, orthorectified, and atmospherically corrected using the empirical line calibration method [21].

Eight cloud-free Formosat-2 images were available over the study area during the 2013 growing season (Table I). The Formosat-2 imagery was geo-referenced and co-registered to the UAV imagery using a high-resolution aerial photograph. All imagery was converted to reflectance factors using the parameters in the Formosat-2 metadata files. Light and dark pseudo-invariant pixels were identified in the entire scene by selecting pixels with the least reflectance variation in all the images. These pixels were used to normalize all images to the reflectance of the June 6th Formosat-2 image. The Formosat-2 images were then clipped to the extent of the study area, and a radiometric normalization was applied between the Formosat-2 and UAV imagery. The UAV imagery taken between June 6th and July 17th were convolved to the Formosat-2 spectral bands using the Formosat-2 spectral response function [22] and radiometrically normalized.

The STRS in the current application was constructed at experimental plot level. Therefore, the average spectral reflectance of each experimental plot was calculated for all UAV and Formosat-2 images. Field reflectance measurements using the Cropscan MSR16R were also averaged for each experimental plot.

C. Bayesian Imputation of Formosat-2 Spectra

A priori information regarding the spectra of endmembers within the scene was obtained by creating a spectral library listing all the UAV spectral reflectance factors in the four available images. The study area consists of a potato field where the endmembers within the image series range from soil to green vegetation at various growth stages. It is assumed that the surface spectra within the extent of the STRS are represented within the available UAV imagery. This spectral library was convolved using the Formosat-2 normalized spectral response curve to obtain four spectral “bands” comparable to the Formosat-2 reflectances.

For each experimental plot and each Formosat-2 image, the 100 UAV spectra with the lowest absolute difference to the Formosat-2 spectra were selected from the convolved spectral

library. The average, standard deviation, and covariance were calculated for each of the hyperspectral UAV bands of these 100 samples, and used as the prior for the Bayesian imputation. Selecting the *a priori* information separately for each experimental plot allows the imputed spectra to represent spatial and temporal variation i.e., differences between plots with low vegetation growth and a closed canopy, allowing for a more accurate imputation.

D. Spectral–Temporal Interpolation

Three STRSs were created to illustrate the added value of the proposed method. This first method is similar to the STRS methods studied by [18] and will be referred to as “Direct.” It applied a cubic-spline interpolation to the Formosat-2 and UAV observations, thus interpolating simultaneously along spectral and temporal dimensions. The second method, which will further be referred to as “Two-step,” first imputed the Formosat-2 spectra along the spectral dimension (as in Section II.A.) and then applied a spline interpolation along the temporal dimension. This is similar to [17], although they applied a spline interpolation along the spectral dimension rather than utilizing Bayesian imputation. In the current scenario, the Bayesian imputation is applied first, as differences in spectral characteristics between the two image sources is much larger than the ones in [17]. Third, the Bayesian STRS applied the method described in Section II, consisting of spectral imputation followed by temporal inference. The uncertainty of the Formosat-2 and UAV images (σ_y) was defined as the RMSE between the plot reflectances obtained from the imagery and those obtained from the field data on June 6th and July 17th. The prior uncertainty σ_x was determined empirically by maximizing the correlation between the STRS resulting from a defined σ_x to the field data on the same two dates.

One STRS using each of the three methods was created for all 24 experimental plots. The optimized soil-adjusted vegetation index (OSAVI) (14) [24] and modified chlorophyll absorption in reflectance index (MCARI) (15) [24] were obtained from the STRS for all nine dates with corresponding field measurements. OSAVI is a structural index related to LAI, whereas MCARI is a hyperspectral index related to canopy biochemical parameters e.g., chlorophyll. Both of these have previously shown strong relations to yield variability [25]

$$\text{OSAVI} = [1.16 * (\rho_{800} - \rho_{670})] / [\rho_{800} + \rho_{670} + 0.16] \quad (14)$$

$$\text{MCARI} = [(\rho_{700} - \rho_{670}) - 0.2(\rho_{700} - \rho_{550})] * [\rho_{700} / \rho_{670}] \quad (15)$$

The correlations between the vegetation indices obtained from the STRSs and 1) the same vegetation index at field level; 2) the LAI measured at field level; and 3) the canopy chlorophyll measurements were calculated. A linear regression was constructed between the canopy chlorophyll field measurements and STRS MCARI values on corresponding dates. The coefficients obtained through these regressions were applied to the STRS to obtain daily canopy chlorophyll estimates.

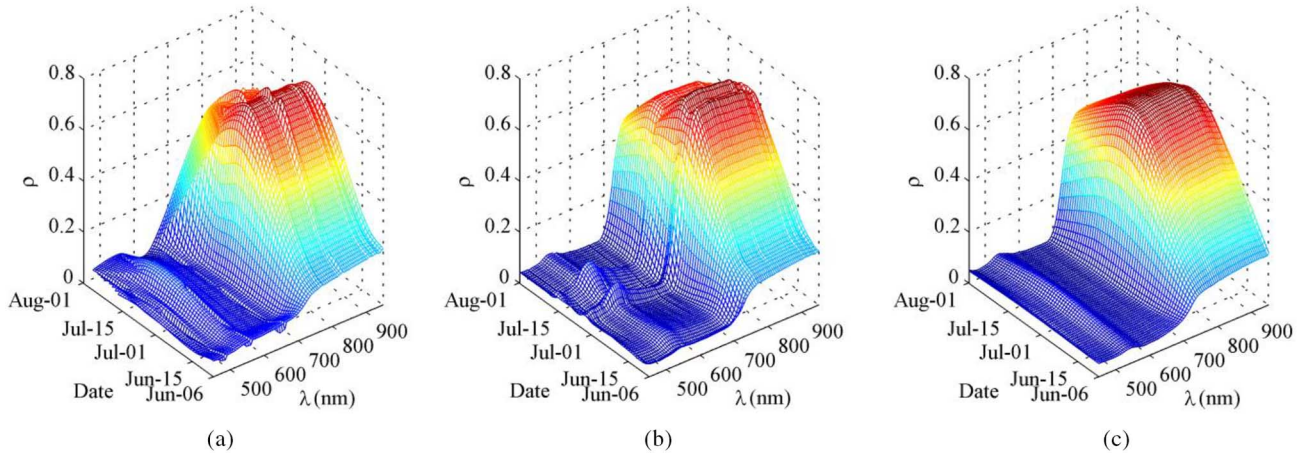


Fig. 2. STRS of experimental plot one created by (a) direct spectral-temporal interpolation; (b) first imputing the Formosat-2 spectra and then performing a temporal spline interpolation; and (c) proposed Bayesian approach including sensor uncertainties.

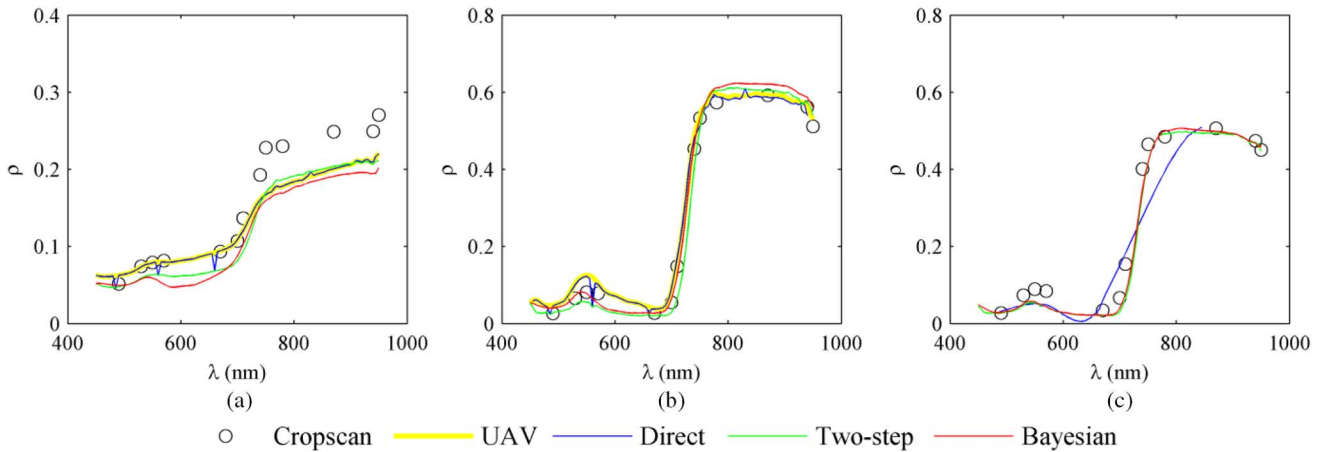


Fig. 3. Comparison of STRS, Cropscan, and UAV spectra on different stages of crop growth period. (a) Open canopy on June 6th. (b) Closed canopy on July 17th. (c) Closed canopy on July 31st when no UAV imagery is available.

IV. RESULTS AND DISCUSSION

The constructed STRSs were 4-D datasets providing daily vegetation spectra with 101 bands for each experimental plot. The STRS of experimental plot 1 using each of the three methods are presented in Fig. 2, while the rest of the plots obtained similar results which are not shown here. The limitations of the Direct method are demonstrated in Fig. 2(a). The last UAV image is on July 17th, whereas Formosat-2 imagery was still available for July 22nd and August 2nd. However, the Formosat-2 imagery only has spectral bands at 660 and 830 nm. The Direct method therefore “flattens” the spectra at the end of July, losing the characteristic red-edge of vegetation reflectance. This is also illustrated in Fig. 3(c).

The two-step method retains the traditional spectral characteristics of vegetation [Fig. 2(b)]. However, the temporal spline interpolation causes spectra to change rapidly in short time periods. For example, the Formosat-2 reflectance factors on July 8th and July 18th are lower than the UAV reflectance factors on July 5th and July 17th, respectively. The sharp decrease between the UAV and subsequent Formosat-2 observations causes the two

TABLE II
CORRELATION COEFFICIENT AND RMSE BETWEEN REFLECTANCES
OBTAINED FROM THREE STRS METHODS AND THE REFERENCE
CROPSCAN SPECTRA

Indicator	Direct spline	Impute + spline	Bayesian approach
RMSE	0.047	0.039	0.032
r	0.923*	0.947*	0.953*

N = 2808, P < 0.001 marked by *.

peaks in green reflectance (~ 560 nm) at these dates. In contrast, the new Bayesian STRS methodology presents realistic daily spectra with smoother temporal changes in Fig. 2(c).

The RMSE and r between the STRS and Cropscan data also indicate that the proposed Bayesian approach performs better than the other two methods (Table II). It is important to note that field data acquisition methods may partly explain discrepancies between STRS and Cropscan spectra. For example, on June 6th the potato plants were not fully grown, and the canopy was still open. The Cropscan apparatus was directed at the

TABLE III
CORRELATION COEFFICIENT BETWEEN VEGETATION INDICES OBTAINED
FROM STRS AND FIELD MEASUREMENTS

VI	Field data	Direct spline	Impute + spline	Bayesian approach
OSAVI	Field OSAVI	0.816*	0.794*	0.820*
	LAI	0.836*	0.836*	0.824*
	Canopy Chl	0.753*	0.717*	0.711*
MCARI	Field MCARI	0.395*	0.193*	0.444*
	LAI	0.265*	0.506*	0.830*
	Canopy Chl	0.091	0.532*	0.774*

N = 216; P < 0.001 marked by *.

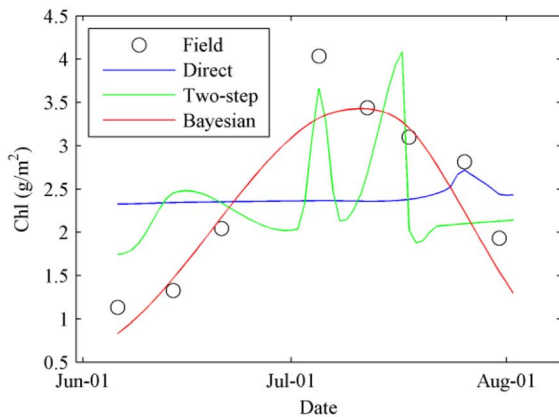


Fig. 4. Temporal profiles of canopy chlorophyll content on experimental plot one, estimated from STRS MCARI values using coefficients estimated from a linear regression between STRS MCARI and field canopy chlorophyll measurements on reference dates.

potato plant, whereas the UAV and Formosat-2 images consist of mixed pixels and are influenced by the soil background. This explains why the UAV spectra, and consequently the STRS spectra are lower than the CropScan data on this date [Fig. 3(a)]. These differences are no longer visible once the canopy has closed [e.g. Fig. 3(b) and (c)]. This discrepancy is especially important when using vegetation indices which are sensitive to soil background effects, e.g., red-edge position (REP).

The correlations between the OSAVI obtained through the STRS and the field data are similar for all three methods tested (Table III). The Direct method provides slightly higher correlations to the LAI and canopy chlorophyll than the Bayesian STRS, which could be due to an overestimation of the sensor uncertainties. Further research could analyze methods to estimate the uncertainty of satellite measurements. However, the MCARI obtained through the Bayesian approach has a higher correlation to LAI and canopy chlorophyll than the other two methods. This is likely due to the fact that the wavelengths which are utilized in the vegetation indices. The OSAVI is based on surface reflectance at 670 and 800 nm, which fall within the range of Formosat-2 spectral bands. The MCARI, however, utilizes surface reflectance data at 700 nm, which is not present in Formosat-2 imagery. It is therefore highly dependent on the interpolation method used. This is also evident in Fig. 4, which indicates that the Bayesian STRS method more

accurately captures the crop phenological status represented by the canopy chlorophyll content based on the MCARI.

V. CONCLUSION

This paper presents a new approach to construct a 4-D STRS, which contains continuous surface reflectance data along both spectral and temporal dimensions. The Bayesian STRS approach obtained a lower RMSE (0.032) and higher correlation (0.953) to spectral measurements at field levels than two alternative STRS methods based on previous studies [17], [18]. The new method also has a considerably more accurate estimation of MCARI, a vegetation index based on wavelengths outside the extent of Formosat-2 imagery. These findings are very important for future STRS applications, as it indicates that constructing an STRS based on the proposed Bayesian method can accurately interpolate a limited number of hyperspectral measurements to daily observations during an entire growing season. Future applications of STRS should consider that the increased precision of narrowband indices obtained from the STRS should compensate for the additional uncertainty induced by spectral-temporal interpolation techniques when compared to direct broadband observations—as is the case with canopy chlorophyll in the current study.

This study demonstrates the possibility of accurately combining multispectral and hyperspectral data, along both spectral and temporal dimensions through a Bayesian approach to STRS. Future studies could combine additional sensors, providing surface reflectance data at the spectral and temporal intervals defined by the user. In applications such as precision farming, it could help bridge the gap between sensor capabilities and data requirements.

ACKNOWLEDGMENT

The authors would kindly like to thank Dr. C.-C. Liu of National Cheng Kung University for providing us with the Formosat-2 spectral response data.

REFERENCES

- [1] R. Gebbers and V. I. Adamchuk, "Precision agriculture and food security," *Science*, vol. 327, no. 5967, pp. 828–31, Feb. 2010.
- [2] D. J. Mulla, "Twenty five years of remote sensing in precision agriculture: Key advances and remaining knowledge gaps," *Biosyst. Eng.*, vol. 114, no. 4, pp. 358–371, Apr. 2013.
- [3] D. Haboudane, J. R. Miller, N. Tremblay, P. J. Zarco-Tejada, and L. Dextraze, "Integrated narrow-band vegetation indices for prediction of crop chlorophyll content for application to precision agriculture," *Remote Sens. Environ.*, vol. 81, no. 2–3, pp. 416–426, Aug. 2002.
- [4] J. G. P. W. Clevers and L. Kooistra, "Using hyperspectral remote sensing data for retrieving canopy chlorophyll and nitrogen content," *IEEE J. Sel. Top. Appl. Earth Observ. Remote Sens.*, vol. 5, no. 2, pp. 574–583, Apr. 2012.
- [5] D. A. Sims and J. A. Gamon, "Relationships between leaf pigment content and spectral reflectance across a wide range of species, leaf structures and developmental stages," *Remote Sens. Environ.*, vol. 81, no. 2–3, pp. 337–354, Aug. 2002.
- [6] J. Delegido *et al.*, "A red-edge spectral index for remote sensing estimation of green LAI over agroecosystems," *Eur. J. Agron.*, vol. 46, pp. 42–52, Apr. 2013.

- [7] R. Main *et al.*, "An investigation into robust spectral indices for leaf chlorophyll estimation," *ISPRS J. Photogramm. Remote Sens.*, vol. 66, no. 6, pp. 751–761, Nov. 2011.
- [8] J. A. J. Berni, S. Member, P. J. Zarco-tejada, L. Suárez, and E. Fereres, "Thermal and narrowband multispectral remote sensing for vegetation monitoring from an unmanned aerial vehicle," *IEEE Trans. Geosci. Remote Sens.*, vol. 47, no. 3, pp. 722–738, 2009.
- [9] C. Zhang and J. Kovacs, "The application of small unmanned aerial systems for precision agriculture: a review," *Precis. Agric.*, vol. 13, no. 6, pp. 693–712, Jul. 2012.
- [10] J. Suomalainen *et al.*, "A lightweight hyperspectral mapping system with and photogrammetric processing chain for unmanned aerial vehicles," *Remote Sens.*, vol. 6, no. 11, pp. 11013–11030, 2014.
- [11] A. Bégué, P. Todoroff, and J. Pater, "Multi-time scale analysis of sugarcane within-field variability: improved crop diagnosis using satellite time series?," *Precis. Agric.*, vol. 9, no. 3, pp. 161–171, Apr. 2008.
- [12] H. Yao and Y. Huang, "Remote sensing applications to precision farming," in *Remote Sensing of Natural Resources*. New York, NY, USA: CRC Press, 2013, pp. 333–352.
- [13] D. P. Roy *et al.*, "Multi-temporal MODIS–Landsat data fusion for relative radiometric normalization, gap filling, and prediction of Landsat data," *Remote Sens. Environ.*, vol. 112, no. 6, pp. 3112–3130, Jun. 2008.
- [14] C. M. Gevaert and F. J. García-Haro, "A comparison of STARFM and an unmixing-based algorithm for Landsat and MODIS data fusion," *Remote Sens. Environ.*, vol. 156, pp. 34–44, Jan. 2015.
- [15] J. Amorós-López *et al.*, "Multitemporal fusion of Landsat/TM and ENVISAT/MERIS for crop monitoring," *Int. J. Appl. Earth Observ. Geoinf.*, vol. 23, pp. 132–141, Aug. 2013.
- [16] D. Fasbender, J. Radoux, and P. Bogaert, "Bayesian data fusion for adaptable image pansharpening," *IEEE Trans. Geosci. Remote Sens.*, vol. 46, no. 6, pp. 1847–1857, Jun. 2008.
- [17] G. Villa *et al.*, "Spectro-temporal reflectance surfaces: a new conceptual framework for the integration of remote-sensing data from multiple different sensors," *Int. J. Remote Sens.*, vol. 34, no. 9–10, pp. 3699–3715, May 2013.
- [18] M. Mello *et al.*, "STARS: A new method for multitemporal remote sensing," *IEEE Trans. Geosci. Remote Sens.*, vol. 51, no. 4, pp. 1897–1913, Apr. 2013.
- [19] K. Murphy, *Machine Learning: A Probabilistic Perspective*. Cambridge, MA, USA: MIT Press, 2012, p. 1098.
- [20] I. Mariotto, P. S. Thenkabail, A. Huete, E. T. Slonecker, and A. Platonov, "Hyperspectral versus multispectral crop-productivity modeling and type discrimination for the HypsIRI mission," *Remote Sens. Environ.*, vol. 139, pp. 291–305, Dec. 2013.
- [21] J. Uddling, J. Gelang-Alfredsson, K. Piikki, and H. Pleijel, "Evaluating the relationship between leaf chlorophyll concentration and SPAD-502 chlorophyll meter readings," *Photosynth. Res.*, vol. 91, no. 1, pp. 37–46, Jan. 2007.
- [22] L. Kooistra *et al.*, "Crop monitoring using a light-weight hyperspectral mapping system for unmanned aerial vehicles: first results for the 2013 season," in *Proc. Workshop UAV-Based Remote Sensing Methods Monit. Veg.*, Apr. 2014, pp. 51–58.
- [23] C. C. Liu *et al.*, "Vicarious calibration of the Formosat-2 remote sensing instrument," *IEEE Trans. Geosci. Remote Sens.*, vol. 48, no. 4, pp. 2162–2169, Apr. 2010.
- [24] G. Rondeaux, M. Steven, and F. Baret, "Optimization of soil-adjusted vegetation indices," *Remote Sens. Environ.*, vol. 55, no. 2, pp. 95–107, Feb. 1996.
- [25] C. Daughtry, C. L. Walthall, M. S. Kim, E. Brown de Colstoun, and J. E. I. McMurtrey, "Estimating corn leaf chlorophyll concentration from leaf and canopy reflectance," *Remote Sens. Environ.*, vol. 74, no. 2, pp. 229–239, Nov. 2000.
- [26] P. J. Zarco-Tejada, S. L. Ustin, and M. L. Whiting, "Temporal and spatial relationships between within-field yield variability in cotton and high-spatial hyperspectral remote sensing imagery," *Agron. J.*, vol. 97, no. 3, p. 641, 2005.



Caroline M. Gevaert received the M.Sc. degree in remote sensing from the University of Valencia, Valencia, Spain, and the M.Sc. degree in geographic information science from Lund University, Lund, Sweden. She is currently pursuing the Ph.D. degree at the Earth Observation Science Department of the Faculty ITC, University of Twente, Enschede, The Netherlands.



Juha Suomalainen received the Ph.D. degree in physics from the University of Helsinki, Helsinki, Finland, in 2012.

He is currently a Post-Doctoral Researcher with the Laboratory of Geo-Information Science and Remote Sensing, University of Wageningen, Wageningen, The Netherlands. His research interests include unmanned aerial vehicle-based remote sensing, optical measurement system, and interaction of light with natural targets.



Jing Tang received the Ph.D. degree from Lund University, Lund, Sweden. Her thesis focused on investigating distributed hydrological processes interactions with vegetation distribution and carbon cycling in high-latitude regions.

She currently works as a Postdoc with Lund University and mainly focus on linking the dynamics of soil water dissolved organic carbon (DOC) concentrations with vegetation types and hydrological transports. Furthermore, she will soon work at the Copenhagen University and focus on exploring

what controls emission of biogenic volatile organic compounds under changing climate.



Lammert Kooistra received the M.Sc. degree in soil science from Wageningen University, Wageningen, The Netherlands, and the Ph.D. degree from the Radboud University, Nijmegen, The Netherlands. The subject of his dissertation was incorporating spatial variability in ecological risk assessment of contaminated river floodplains.

He is currently working as an Assistant Professor with Wageningen University, Wageningen, The Netherlands. He has authored more than 25 peer-reviewed journal papers. His research interests

include application of integrated sensing technology for (agro)environmental conservation and management with special interest in combining imaging spectroscopy, sensor networks, and ecological modeling.